# QUALITATIVE LIF IMAGING OF OH AND NO IN TURBULENT PILOTED FLAMES OF CNG AND CNG-$O_2$ FUELS

**M. Juddoo* and A.R. Masri***
mrinal.juddoo@sydney.edu.au
*School of Aerospace, Mechanical and Mechatronic Engineering,
The University of Sydney, NSW 2006, Australia

## Abstract
This paper presents qualitative but novel measurements of LIF-OH and LIF-NO in turbulent, non-premixed pilot-stabilized flames at various departures from blow-off. The novelty lies in investigating pure compressed natural gas (CNG) as well as a mixture of CNG/oxygen = 9/1 by volume. Comparative profiles of OH and NO signals are presented for various axial locations within the flames. It is shown that with increasing jet velocity, and as the flames approach blow-off, the peak levels of OH and NO decrease at varying degrees depending on the axial location within the flame. The decrease is most significant around x/D=20 where the turbulence-chemistry interactions are most intense but reduces upstream due to the influence of the pilot. Further downstream at x/D=30, the OH peak levels show some recovery due to reduced mixing rates but the same is not observed for NO. Increasing the oxygen content leads to increased peak levels in both OH and NO.

## Introduction
Turbulent piloted non-premixed and partially premixed jet flames continue to be an excellent platform for investigating various aspects of turbulence-chemistry interactions and for developing and validating modelling approaches [1]. A range of fuel mixtures have been explored to date including methane (or compressed natural gas, CNG) [2-4], methanol [5] and mixtures of CO-$H_2$-$N_2$ fuels [6]. Although the first studies of this burner used pure methane (or CNG) as fuel [2], later measurements shifted to partially premixed mixtures of $CH_4$-air (=1/3 by volume) [3-4, 7-9] with the intention of broadening the reaction zone width and increasing the stoichiometric mixture fraction to shift the reaction zone closer to the shear layer of the jets.

Recently, and using the same piloted burner, turbulent flames of CNG partially-premixed with different levels of oxygen were studied [10]. The addition of oxygen to the fuel increases the flames temperature, as well as stoichiometric mixture fraction and broadens the reaction zone. It was found that, for the same conditions in the pilot, the stability limits of the flames improve almost linearly with addition of oxygen (up to about 30% by volume) to the fuel. High-speed imaging of LIF-OH [10] was performed on a range of these flames, as well as others [11-13] at various departures from blow-off. These time sequenced images revealed novel information about the mechanisms of formation of extinction and re-ignition events. It was found that the "breakages/extinction" of reaction zones occur at faster rates than the occurrence of "closures/re-ignition". Re-ignition is also largely due to the reacting kernels that propagate from upstream and re-institute a stable flame further downstream where the conditions are more are favorable.

Pure methane or CNG flames have received little attention since the early inception of the piloted flame burner. The database for these flames generated in the mid nineteen-eighties remains relevant and challenging albeit limited to measurements of temperature and stable species. Current numerical approaches are still incapable of adequately computing the structure of these flames close to blow-off and this is essentially due to the difficulties associated with the narrow reaction zones resulting from flames of pure CNG or methane. It was recently shown that the RANS-PDF approach coupled with the EMST mixing model fails to predict finite rate chemistry effects for fuels with narrow reaction zones and this is largely limited by the inadequacy of the mixing models [14]. More advanced approaches using large eddy simulation with either multiple mapping closure (MMC) [15-16], conditional moment closure (CMC) methods [17-19] or flamelets progress variable models [20] may have better potential at computing flames with narrow reaction zones.

In anticipation of renewed interests in turbulent piloted flames of pure CNG or methane, this papers revisits these flow conditions and presents comparative joint imaging of LIF-OH and LIF-NO (at a repetition rate of 10Hz) in flames L, B and M which have decreasing departures from blow-off [2]. Additionally, flames partially premixed with 10% oxygen (CNG-$O_2$ = 9-1 by volume) are also investigated over a range of jet velocities. Although the images are qualitative, they reveal interesting features about the effects of finite rate chemistry and the addition of oxygen on these two key species.

**Experimental Setup**

The UV beam for the OH-LIF is generated using the 2nd Harmonic of a seeded SpectraPhysics PRO-350 Nd:YAG pumping a SIRAH PrecisionScan dye laser. Rhodamine 6G diluted in ethanol is used as the lasing medium and produces a fundamental beam at 566nm which is then frequency doubled in a Beta-Barium Borate (BBO) crystal to produce UV radiation at 283.1nm, predominantly corresponding to the $Q_1(6)$ excitation for the $A^2\Sigma^+ \rightarrow X^2\Pi$ (1,0) system of OH. The UV beam is spectrally purified by using a set of four Pellin-Broca prisms before being focused at the probe volume through a 300mm focal length plano-convex fused silica lens. The collection optics consisted of a UV 105mm Nikkor $f_{\#}4.5$ lens coupled to an 18mm 3rd Generation UV sensitive intensifier. The lens-intensifier setup is subsequently coupled to a CCD (LaVision Imager Intense) camera using two Nikkor 50mm $f_{\#}1.2$ lenses which are coupled back-to-back. Resonant UV light and flame luminosity is rejected using a narrowband filter centered at 313nm with a 10nm FWHM bandwidth combined with a 1μs gate time on the intensifier multi-channel plate (MCP). The fluctuation of the 283nm beam is monitored by projecting a small portion of the beam onto the front surface of the intensifier, by using a fibre-optic cable. Fluctuations in both the intensifier and the laser energy can consequently be measured and corrected for. A schematic diagram of the experimental setup can be found in Fig. 1.

The UV beam for the NO-LIF is generated using the 2nd Harmonic of a seeded SpectraPhysics PRO-350 Nd:YAG pumping a SIRAH PrecisionScan dye laser using DiChloroMethane (DCM) in ethanol as the lasing medium. The dye laser fundamental beam generated at 622nm is then sum frequency mixed with a 355nm beam from the 3rd Harmonic of the Nd:YAG laser, through a BBO crystal to produce a UV beam at 226.03nm, corresponding predominantly to the $Q_1(14)$ excitation line for the $A \rightarrow X$ (0,0) system of NO. The UV beam is spectrally isolated using a set of four Pellin-Broca prisms. The detection system for the NO-LIF signal consists of two sets of LAPQ/APMQ (CVI Products) lenses coupled back to back to produce a combined $f_{\#}1.65$ and a clear aperture of 60mm. The lenses are focused onto a 3rd Generation UV sensitive image intensifier, which in turn is lens-coupled to a CCD (LaVision Imager Intense) camera via two Nikkor 50mm $f_{\#}1.2$ lenses. Resonant UV light, flame luminosity and the 283nm scattering is completely rejected using a

narrowband filter centered at 236nm with a 10nm FWHM bandwidth and with a 1μs gate width on the image intensifier. The filter is designed specifically for the purpose of rejecting all resonant light at 226nm as well. It has an optical density of over 5 at 226nm, ensuring total rejection of resonant fluorescence, and has a peak transmission of 59% at 236nm. The fluctuation of the 226nm beam is monitored by projecting a small portion of the beam onto the front surface of the intensifier, by means of a fibre-optic cable. Fluctuations in both the intensifier and the laser energy can consequently be measured and corrected for.

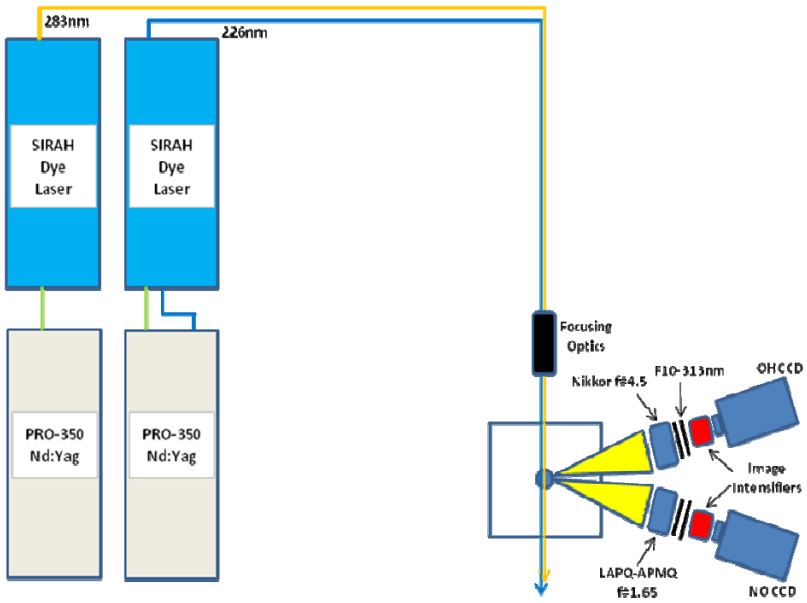


**Figure 1**. Experimental Setup

**The Burner**

The piloted burner used in the current study has the same dimensions as the one used in earlier studies [5-6, 21] and has a stainless-steel central jet of 7.2mm (inner diameter), 950mm long and a wall thickness of 0.25mm. The pilot flame has a mixture of acetylene, hydrogen and air flowing through the annulus and has a carbon to hydrogen ratio adjusted to that of the fuel in the central jet. The outer annulus diameter is 18.9mm with wall thickness of 0.35mm. The pilot flame holder has a total of 72 premixed flames aligned in three rows of 0.9, 1.0 and 1.1mm diameter holes, and the holder sits 4mm upstream of the nozzle exit. Three parameters control the overall flame characteristics namely the pilot burnt gas velocity, $\bar{u}_{pb}$, the bulk jet velocity, $\bar{u}_j$, and the mean external air velocity $\bar{u}_e$ as outlined in [6].

The burner is centrally aligned in a vertical wind tunnel, which has an exit plane of 150x150mm and the working station in unconfined. Wire mesh screens have been placed at various locations in the plenum chamber to provide a smooth co-flowing air stream with very low turbulence intensity and the wind tunnel fan is driven by a variable speed motor with feedback control to ensure a constant fan speed and air flow.

The flow-rates of all reactants were monitored using Fischer and Porter tri-flat tubes and rotameters with an accuracy of ±2% of the full scale. CNG is used as the main fuel and its volumetric composition is 88.8% $CH_4$, 7.8% $C_2H_2$, 1.9% $CO_2$ and 1.2%$N_2$ with the remaining 0.3% being a mixture of propane, propene, butane and pentanes. In the flow-rate calculations, CNG is taken as 100% $CH_4$ with the minor constituents neglected.

**Selected Flames**

Extensively studied Sydney University CNG flames L, B and M [2, 6] are used in this study and are at 60, 70 and 80% of their blow-off velocity ($\bar{u}_{BO}$ = 68m/s) respectively and have a stoichiometric mixture fraction, $\xi_s$=0.055. The oxygen variant consists of CNG/$O_2$ mixture, where pure CNG is partially-premixed with 10% oxygen. Since these flames are variants of the original piloted cases L, B and M, they are run at the same percentage of their blow-off limit and labelled similarly but with an indication of the amount of oxygen used in the fuel mixture. For example flame B10 uses a mixture of 10% $O_2$ and 90% CNG (by volume). The blow-off limit of the CNG-$O_2$ (9:1) mixture was determined experimentally ($\bar{u}_{BO}$ = 79m/s). Details of the selected flames are given in Table 1.

**Table 1.** Selected Flames and Relevant Parameters.

| Flame Code | $\bar{u}_j$ (m/s) | $\bar{u}_j / \bar{u}_{BO}$ | Mole Fraction | | $\xi_s$ | Re |
|---|---|---|---|---|---|---|
| | | | CNG | $O_2$ | | |
| **L** | **41.0** | **60.3%** | **1** | **0** | **0.055** | **17900** |
| **B** | **48.0** | **70.6%** | **1** | **0** | **0.055** | **20400** |
| **M** | **55.0** | **80.9%** | **1** | **0** | **0.055** | **23800** |
| **L10** | **48.2** | **60.3%** | **0.9** | **0.1** | **0.070** | **21000** |
| **B10** | **56.5** | **70.6%** | **0.9** | **0.1** | **0.070** | **24100** |
| **M10** | **64.7** | **80.9%** | **0.9** | **0.1** | **0.070** | **27800** |

**Laminar Flame Calculations**

A series of laminar flame calculations are performed using the open source code CANTERA [22] and presented in Figs. 2 and 3. The code solves a one-dimensional counter-flow diffusion flame in an opposed jet configuration and is run as a script in MATLAB [23]. Detailed chemistry using the GRI3.0 mechanism [24] together with multi-component diffusion transport properties is used in all calculations and radiation losses are not included. Three different cases are considered, where the first consists of having pure methane as fuel, and the other two cases second involve methane that is enriched with 10% and 20% oxygen by volume.

Computed profiles of the OH and NO mole fractions are shown, respectively in Figures 2 and 3 for the three different fuel mixtures ($CH_4$, $CH_4/O_2$ =9/1 and $CH_4/O_2$ =8/2, volumetric ratio). All results are presented versus mixture fraction for a strain rate of $\alpha$=120$s^{-1}$. The peak OH mole fraction shows an increase with the added oxygen and the OH profile broadens, indicating a wider reaction zone in the mixture zone in mixture fraction space. This is also confirmed by broader profiles of O and H radicals that are not presented here. The peak mole fraction of NO increases from 1.45$e^{-4}$ to 1.79$e^{-4}$ as the oxygen content in the fuel increases from 0% to 10% and the peak NO occurs around the stoichiometric mixture fraction.

Also plotted versus mixture fraction in Figs. 2 and 3 are the calculated quenching rates that would be expected for both OH and NO in the three laminar flames considered here for a single strain rate of $\alpha$=120$s^{-1}$. These calculations use the computed compositional structure and relevant quenching factors for each of OH and NO as obtained by Tamura et. al [25]. It is shown that for OH, the change in the quenching factor with increasing level of oxygenation in the fuel is small and of the order of about 5-15% around the stoichiometric region, which also changes with the fuel from 0.05 for pure methane to 0.07 and 0.09 in mixture fraction space for $CH_4/O_2$ =9/1 and $CH_4/O_2$ =8/2 fuels, respectively. For NO, the change in the quenching levels is more significant on the rich side of stoichiometry especially with increasing oxygen in the fuel, while on the leaner side, the quenching rate only increases by about 2% to 5%

around the stoichiometric region for the flames with 10% and 20% oxygen in the fuel. These quenching corrections are used here to make estimates about the expected trends in the peak measured OH and NO signals.

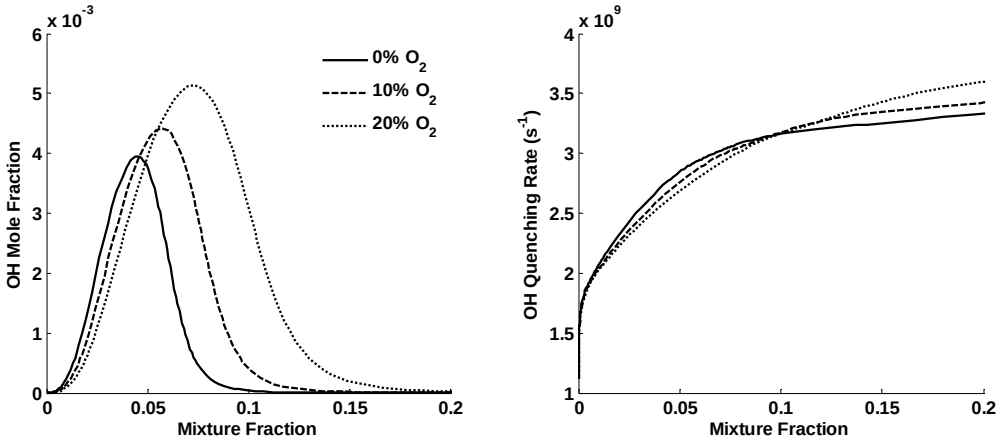


**Figure 2**. Laminar flame calculations for three fuels: $CH_4$, $CH_4/O_2$ =9/1 (by vol.) and $CH_4/O_2$ =8/2 (by vol.) with a strain rate of $\alpha$=120$s^{-1}$ plotted versus mixture fraction. Right: OH mole fraction, Left: OH quenching rate.

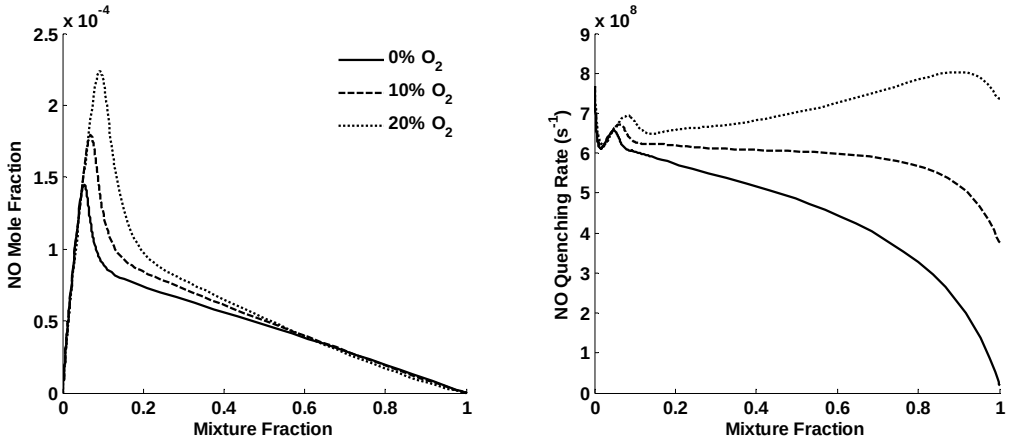


**Figure 3**. Laminar flame calculations for three fuels: $CH_4$, $CH_4/O_2$ =9/1 (by vol.) and $CH_4/O_2$ =8/2 (by vol.) with a strain rate of $\alpha$=120$s^{-1}$ plotted versus mixture fraction. Right: NO mole fraction, Left: NO quenching rate.

A test was carried out on a simple Bunsen diffusion flame to investigate the effects of quenching on the OH-signal collected on the CCD camera as the level of oxygen in the fuel increases from 0% to 15% by volume. Radial profiles of the mean OH-signal intensities measured in the three laminar flames are plotted in Fig. 4 versus an arbitrary radial location (not marked). It is clear that the OH signal does indeed increase with increasing level of oxygen in the fuel. It was shown in Fig. 2 that the quenching correction for OH changes minimally with the level of oxygenation in the fuel. This confirms that the difference in the OH signal intensities shown here is not due to quenching and reflects an actual increase in OH with increasing oxygen content in the fuel. This is consistent with the laminar flame calculations shown earlier (LHS plot of Fig. 2).

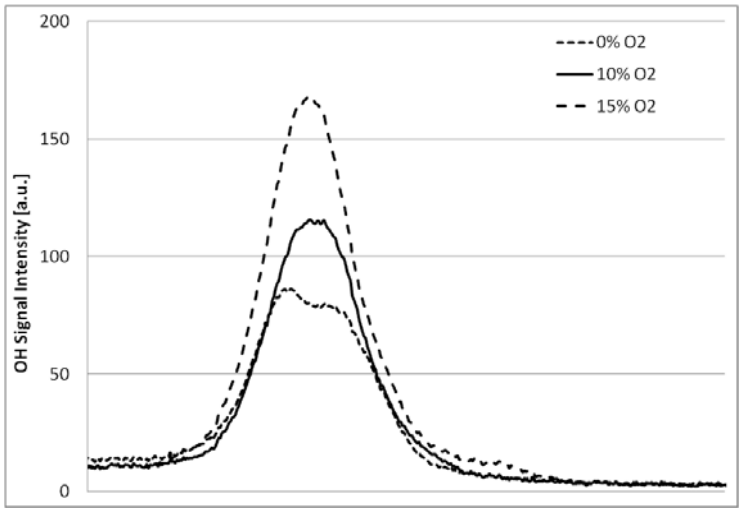


**Figure 4**. Radial profiles of mean OH-signal intensities measured in three laminar flames of $CH_4$, $CH_4/O_2$ =9/1 (by vol.) and $CH_4/O_2$ =8.5/1.5 (by vol.). Note that the axial axis is intentionally left unmarked as it refers to a general radial location in the Bunsen burner where the centreline is on the LHS of the axis.

**Results**

Sample OH and NO images:

Figure 5 shows sample instantaneous images of OH and NO collected at x/D = 10, 20 and 30 in flames B and B10. The false colour contours indicate signal intensity and the jet centerline lies on the RHS of each plot with the arrows pointing to the direction of increasing distance from the centreline. The axial distance spanned by each images is marked on the vertical axis. It is clear that the intensity of the OH signal decreases in the regions at x/D = 20 and 30, mainly due to the strong extinction events occurring. The width of the NO profiles, also tend to broaden downstream. As oxygen is added to the fuel, the OH and NO profiles both show a broadening along with stronger signal intensities compared to the pure fuel cases. It is noted that the NO images are less sharp than those of OH reflecting the higher S/N ratio in the latter measurements.

Profiles of OH- and NO-signal intensity:

Figures 6 and 7 show, respectively, comparative radial profiles of the measured mean signal intensities of OH and NO at various axial locations in the six flames studied here. Each plot shows, for a given axial location, a comparison in the mean signal intensity of either OH or NO plotted versus r/R (R is the jet radius, R=3.6mm) measured in three flames (either L, B, and M or L10, B10, and M10).

The mean OH profiles of flames L, B and M all show a decrease as x/D increases from 10 to 30. At x/D = 10, the flames are still under the influence of the pilot, hence the high OH levels observed at this location. Flame M shows the sharpest decrease in OH levels downstream since it is the closest to its blow-off limit and strong extinction events occur around x/D = 20 and 30. This result is also confirmed by the temperature scatter plot [6] at these locations as obtained from previous investigations of these flames performed in the late eighties and early nineties [6, 26]. As oxygen is added to the fuel, the stability of the flames increases [14] and re-ignition occurs at x/D = 30 for flames B10 and M10, as shown by the initial decrease in OH levels at x/D = 20 followed by an increase at x/D = 30.

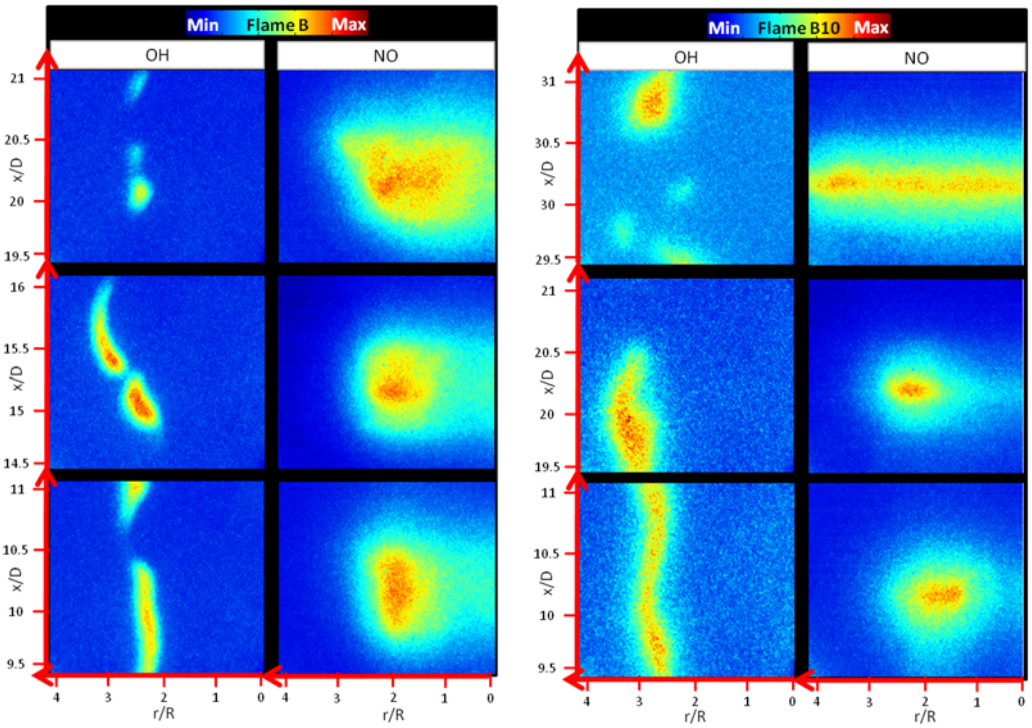


**Figure 5**. Instantaneous OH and NO images in flame B (Left) and flame B10 (Right).

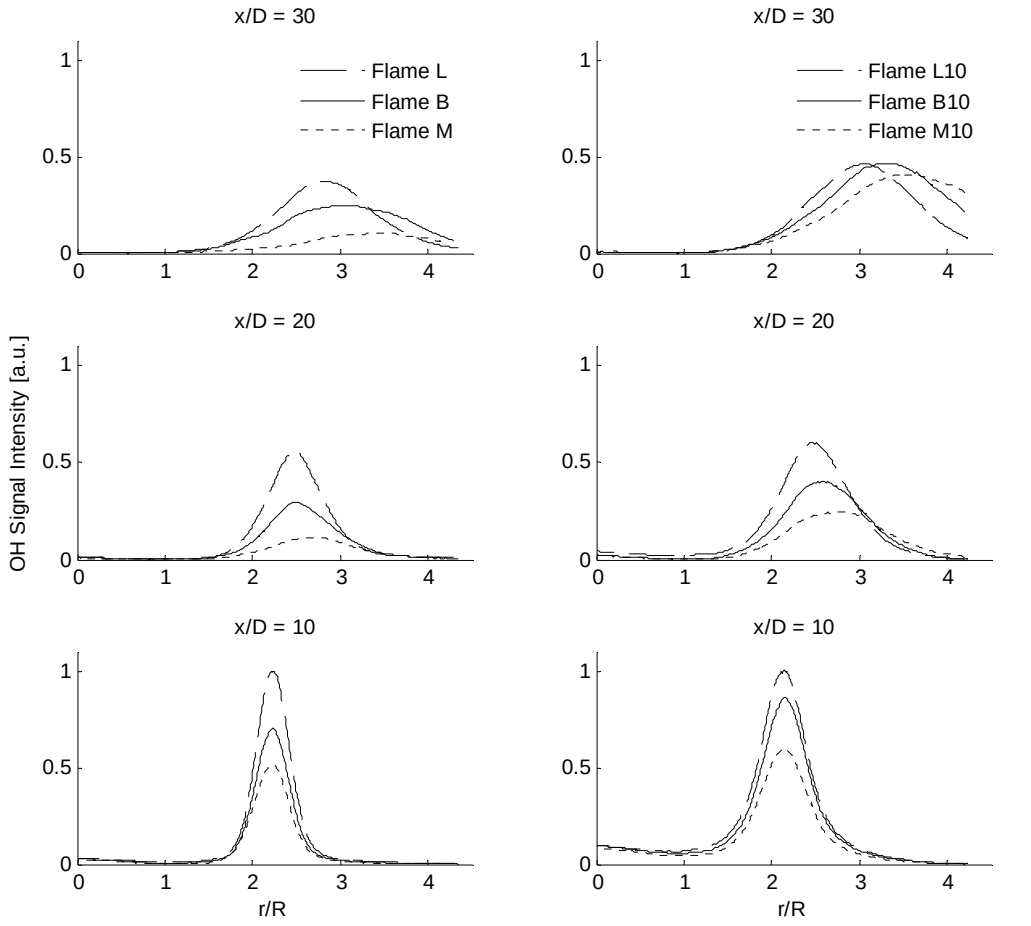


**Figure 6**. Mean radial profiles of measured OH signal intensities at x/D = 10, 20 and 30. Left: Flames L, B and M. Right: Flames L10, B10 and M10.

The mean profiles of NO show almost no change for flame L as x/D increases from 10 to 30. As the jet velocity increases for flames B and M, the levels of NO show a decrease downstream at x/D = 20 and 30 and is due to the higher strain levels in the flames causing a decrease in residence time and lower temperatures, and hence reduced NO formation. As the fuel is oxygenated, an almost identical observation as in non-oxygenated flames is made regarding the NO behavior. As the jet velocity increases, the NO levels show a decrease and less NO is present in the regions where strong extinction events occur such as x/D = 20 and 30. However, the measured peak NO levels are lower for the oxygenated flames compared to the pure CNG flames. Since NO peaks on the rich side of stoichiometry, the quenching rate, shown in Fig. 3, due to the oxygen present in the fuel jet increases significantly and may possibly be causing the reduced signal observed in the oxygenated flames.

The overall trend in the OH and NO behaviour is consistent with previous work carried out by Barlow et. al. [3, 8-9] on a similar burner with $CH_4$-air (1:3) flames, with the exception of upstream locations (<x/D = 10). The discrepancy between the two measurements at these upstream locations lies in the fact that the pilot influence was maintained constant by increasing its respective velocity linearly with the main jet velocity in the $CH_4$-air flame measurements while in the current experiment, the pilot velocity was kept constant throughout, hence, as the jet velocity increases, the heat release contribution of the pilot compared to the main jet decreases.

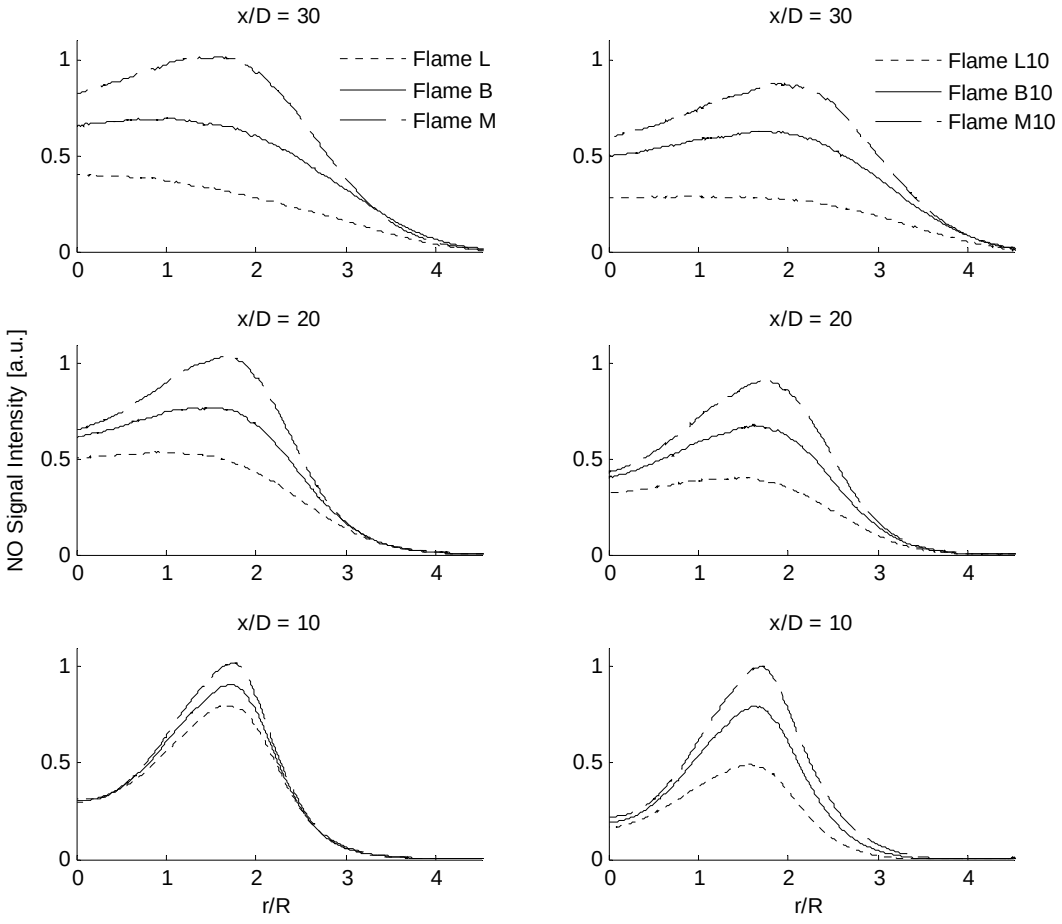


**Figure 7**. Mean radial profiles of measured NO signal intensities at x/D = 10, 20 and 30. Left: Flames L, B and M. Right: Flames L10, B10 and M10.

The measurements of OH and NO presented here, while qualitative in nature, complement the current data for piloted methane (or CNG) flames where detailed information already exists on the compositional structure of stable species. The trends obtained in these flames as they approach extinction pose a challenge to modelers and this is also true for the CNG-oxygen fuel mixtures. Efforts to predict such finite-rate chemistry effects in fuels mixtures with narrow reaction zones is currently a research priority of the turbulent combustion research community.

**Conclusions**

As the jet velocity increases and the flames approach global blow-off, it is found that the peak measured levels of both OH and NO decrease in both the CNG and CNG-$O_2$ flames studied here. The decrease is relatively small close to the jet exit plane (x/D=10) while still under the influence of the pilot but peaks at x/D=20 with differences of more than 50% noted in the peak mean values. Further downstream, at x/D=30, some recovery in OH peak levels is noted due to relaxed mixing rates as shown for flames M10. However, differences in the peak measured levels of NO continue to increase. Laminar flame calculations show that increasing the oxygen content leads to increased peak levels in both OH and NO. The measurements of OH show similar trends for the CNG and the CNG-$O_2$ flames but the same cannot be said for the LIF-NO images due to the strong quenching effects of oxygen on the NO-signal.

**Acknowledgements**

This research is supported by the Australian Research Council (ARC).

**References**

1. TNF, “International Workshop on Measurement and Computation of Turbulent (Non)Premixed Flames ”, available at http://www.sandia.gov/TNF/
2. A. R. Masri, R. W. Bilger, "Turbulent non-premixed flames of hydrocarbon fuels near extinction: mean structure from probe measurements", *Proc. Comb. Inst*, 21:1511-1520 (1988).
3. R. S. Barlow, J. H. Frank, A. N. Karpetis, J. Y. Chen, "Piloted methane/air jet flames: Transport effects and aspects of scalar structure", *Combust. Flame*, 143:433-449 (2005).
4. Robert S. Barlow, Adonios N. Karpetis, "Scalar length scales and spatial averaging effects in turbulent piloted methane/air jet flames", *Proc. Comb. Inst.*, 30:673-680 (2005).
5. A. R. Masri, R. W. Dibble, R. S. Barlow, "The structure of turbulent nonpremixed flames of methanol over a range of mixing rates", *Combust. Flame*, 89:167-185 (1992).
6. A. R. Masri, R. W. Dibble, R. S. Barlow, "The structure of turbulent nonpremixed flames revealed by Raman-Rayleigh-LIF measurements", *Prog. Energy Sci.*, 22:307-362 (1996).
7. A. N. Karpetis, R. S. Barlow, "Measurements of flame orientation and scalar dissipation in turbulent partially premixed methane flames", *Proc. Comb. Inst.*, 30:665-672 (2005).
8. A. N. Karpetis, R. S. Barlow, "Measurements of scalar dissipation in a turbulent piloted methane/air jet flame", *Proc. Comb. Inst.*, 29:1929-1936 (2002).
9. R. S. Barlow, J. H. Frank, "Effects of turbulence on species mass fractions in methane/air jet flames", *Proc. Comb. Inst*, 27:1087-1095 (1998).
10. M. Juddoo, A. R. Masri, "High-speed OH-PLIF imaging of extinction and re-ignition in non-premixed flames with various levels of oxygenation", *Combust. Flame*, 158:902-914 (2011).

11. I. Boxx, C. Heeger, R. Gordon, B. Böhm, M. Aigner, A. Dreizler, W. Meier, "Simultaneous three-component PIV/OH-PLIF measurements of a turbulent lifted, C3H8-Argon jet diffusion flame at 1.5 kHz repetition rate", *Proc. Comb. Inst.*, 32:905-912 (2009).
12. B. Böhm, C. Heeger, I. Boxx, W. Meier, A. Dreizler, "Time-resolved conditional flow field statistics in extinguishing turbulent opposed jet flames using simultaneous highspeed PIV/OH-PLIF", *Proc. Comb. Inst.*, 32:1647-1654 (2009).
13. C. Kittler, A. Dreizler, "Cinematographic imaging of hydroxyl radicals in turbulent flames by planar laser-induced fluorescence up to 5 kHz repetition rate", *Applied Physics B: Lasers and Optics*, 89:163-166 (2007).
14. M. Juddoo, A.R. Masri, S.B. Pope, "Turbulent Piloted Partially-Premixed Flames with Varying Levels of O2/N2: Stability Limits and PDF Calculations", *Comb. Theory Model.*, In Press: (2011).
15. M. Cleary, A. Klimenko, "A Generalised Multiple Mapping Conditioning Approach for Turbulent Combustion", *Flow, Turbulence and Combustion*, 82:477-491 (2009).
16. Yipeng Ge, M. J. Cleary, A. Y. Klimenko, "Sparse-Lagrangian FDF simulations of Sandia Flame E with density coupling", *Proc. Comb. Inst.*, 33:1401-1409 (2011).
17. A. Kronenburg, M. Kostka, "Modelling extinction and reignition in turbulent flames", *Combust. Flame*, 143:342-356 (2005).
18. A. Kronenburg, M. J. Cleary, "Multiple mapping conditioning for flames with partial premixing", *Combust. Flame*, 155:215-231 (2008).
19. P. Vaishnavi, A. Kronenburg, "Multiple mapping conditioning of velocity in turbulent jet flames", *Combust. Flame*, 157:1863-1865 (2010).
20. E. Knudsen, H. Pitsch, "A general flamelet transformation useful for distinguishing between premixed and non-premixed modes of combustion", *Combust. Flame*, 156:678-696 (2009).
21. S. H. Stårner, R. W. Bilger, R. W. Dibble, R. S. Barlow, "Measurements of Conserved Scalars in Turbulent Diffusion Flames", *Comb. Sci. Tech.*, 86:223-236 (1992).
22. CANTERA, "An Object-Oriented Software package for Reacting Flows, Release 1.6.0" (Jan 2005), available at http://www.cantera.org
23. MATLAB, "MATrix-LABoratory created by The MathWorks, Inc. Version 7 (R14) Service Pack 2", available at http://www.mathworks.com
24. G.P. Smith *et al.*, "GRI-MECH 3.0", available at http://www.me.berkeley.edu/gri_mech/
25. Masayuki Tamura, Pamela A. Berg, Joel E. Harrington, Jorge Luque, Jay B. Jeffries, Gregory P. Smith, David R. Crosley, "Collisional Quenching of CH(A), OH(A), and NO(A) in Low Pressure Hydrocarbon Flames", *Combust. Flame*, 114:502-514 (1998).
26. R. W. Dibble, A. R. Masri, R. W. Bilger, "The spontaneous raman scattering technique applied to nonpremixed flames of methane", *Combust. Flame*, 67:189-206 (1987).